

PAPER

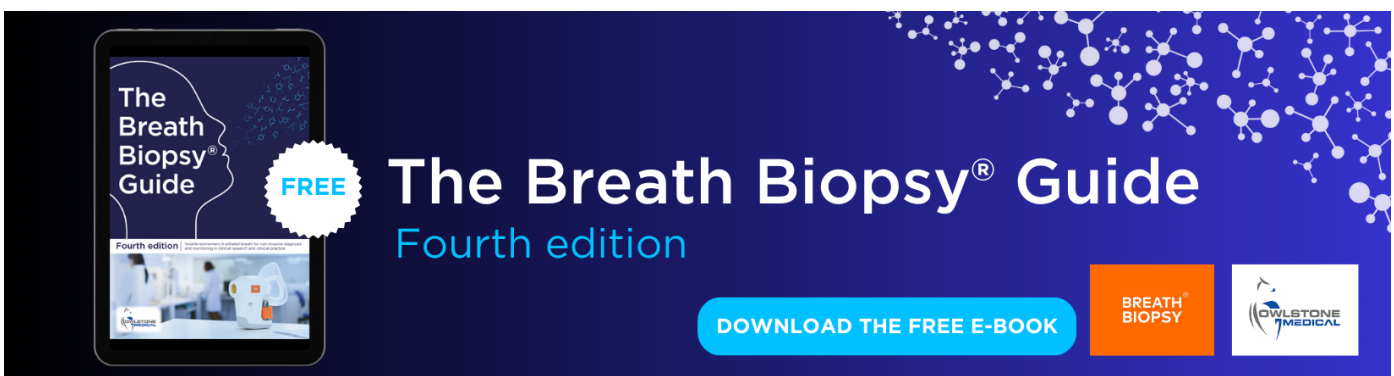
Investigating the physiological mechanisms of the photoplethysmogram features for blood pressure estimation

To cite this article: Wan-Hua Lin *et al* 2020 *Physiol. Meas.* **41** 044003

View the [article online](#) for updates and enhancements.

You may also like

- [Robust blood pressure estimation from finger photoplethysmography using age-dependent linear models](#)
Xiaoman Xing, Zhimin Ma, Mingyou Zhang et al.
- [New photoplethysmogram indicators for improving cuffless and continuous blood pressure estimation accuracy](#)
Wan-Hua Lin, Hui Wang, Oluwarotimi Williams Samuel et al.
- [Reply to Comment on 'New photoplethysmogram indicators for improving cuffless and continuous blood pressure estimation accuracy'](#)
Wan-Hua Lin, Oluwarotimi Williams Samuel and Guanglin Li



The Breath Biopsy® Guide
Fourth edition

FREE

DOWNLOAD THE FREE E-BOOK

BREATH BIOPSY

OWLSTONE MEDICAL



PAPER

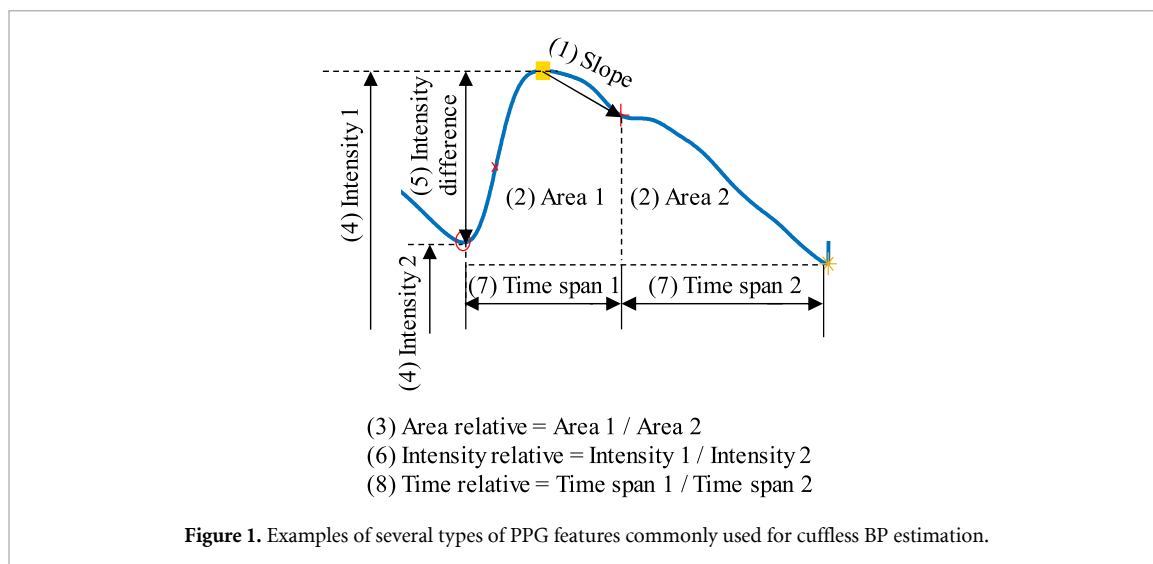
Investigating the physiological mechanisms of the photoplethysmogram features for blood pressure estimation

RECEIVED
20 January 2020REVISED
2 March 2020ACCEPTED FOR PUBLICATION
6 March 2020PUBLISHED
1 May 2020Wan-Hua Lin^{1,2} , Xiangxin Li^{2,3}, Yuanheng Li^{2,3,4}, Guanglin Li^{2,3} and Fei Chen¹ ¹ Department of Electrical and Electronic Engineering, Southern University of Science and Technology, Shenzhen 518055, People's Republic of China² CAS Key Laboratory of Human-Machine Intelligence-Synergy Systems, Shenzhen Institutes of Advanced Technology (SIAT), Chinese Academy of Sciences (CAS), Shenzhen 518055, People's Republic of China³ SIAT Branch, Shenzhen Institute of Artificial Intelligence and Robotics for Society, Shenzhen 518055, People's Republic of China⁴ Zhuhai Campus of Zunyi Medical University, Zhuhai 519000, People's Republic of ChinaE-mail: fchen@sustech.edu.cn**Keywords:** physiological mechanism, blood pressure (BP) estimation, photoplethysmogram (PPG) features, cardiac output (CO), total peripheral vascular resistance (TPR)**Abstract**

Objective: Photoplethysmogram (PPG) signals have been widely used to estimate blood pressure (BP) cufflessly and continuously. A number of different PPG features have been proposed and extracted from PPG signals with the aim of accurately estimating BP. However, the underlying physiological mechanisms of PPG-based BP estimation still remain unclear, particularly those corresponding to various PPG features. In this study, the physiological mechanisms of PPG features for BP estimation were investigated, which may provide further insight. *Approach:* Experiments with cold stimuli and an exercise trial were designed to change the total peripheral vascular resistance (TPR) and cardiac output (CO), respectively. Instantaneous BP and continuous PPG signals from 12 healthy subjects were recorded throughout the experiments. A total of 65 PPG features were extracted from the original, the first derivative, and the second derivative waves of PPG. The significance of the change of PPG features in the cold stimuli phase and in the early exercise recovery period was compared with that in the baseline phase. *Main results:* Intensity-specific PPG features changed significantly ($p < 0.05$) in the cold stimuli phase compared with the baseline phase, demonstrating that they were TPR-correlated. Time-specific PPG features changed significantly ($p < 0.05$) in the early exercise recovery period compared with the baseline phase, suggesting they were CO-correlated. Most of the PPG features associated with slope and area changed obviously both in the cold stimuli phase and in the early exercise recovery period, indicating that they should be TPR-correlated and CO-correlated. *Significance:* The findings of this study explained the intrinsic physiological mechanisms underlying PPG features used for BP estimation, and provided insights for exploring more diagnostic applications of the PPG features.

1. Introduction

Blood pressure (BP) monitoring is important for the diagnosis and prognosis of cardiovascular disease (CVD). Photoplethysmogram (PPG) is the blood perfusion change in the peripheral vasculature which reflects both the cardiac output (CO) and total peripheral vascular resistance (TPR), which are closely associated with BP (Liu *et al* 2014). PPG has been widely used for estimating cuffless and continuous BP in the wearable and telemedicine fields (Kachuee *et al* 2017, Miao *et al* 2017, Slapničar *et al* 2018). Features extracted from the PPG wave could be used alone (Proença *et al* 2019) or in combination with pulse transit time (PTT) to estimate BP (Mukkamala *et al* 2015). In recent years, as the application of machine learning methods shows great potential for better BP estimation (Kachuee *et al* 2017, Miao *et al* 2017, Slapničar *et al* 2018), more PPG features have been explored for accurate BP estimation (Lin *et al* 2018, Ding *et al* 2019).

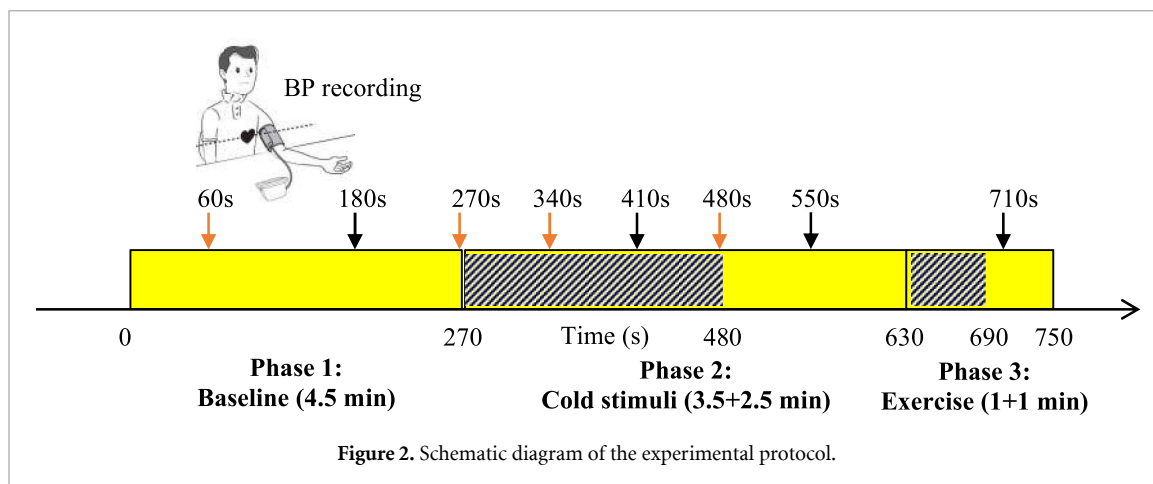


The PPG features commonly used for cuffless BP estimation can be split into eight groups as follows (see figure 1 for typical examples):

- Slope indices: slope between feature points of PPG, such as slope from maximum to dicrotic notch (Kim *et al* 2008) and the rate of wave front increase (Putyatina 2002).
- Area indices: area under the PPG curve between feature points, such as S1, S2, S3, S4 (Kachuee *et al* 2017).
- Area relative indices, such as area ratio of systole to diastole (Li *et al* 2014).
- Intensity indices: intensity at feature point of PPG, such as accelerated plethysmography's peak (Fukushima *et al* 2013).
- Intensity difference indices: intensity difference between feature points, such as ascending intensity difference and descending intensity difference (Lin *et al* 2018).
- Intensity relative indices, such as the ratio of PPG peak intensity to PPG valley intensity (Ding *et al* 2016).
- Time span indices: time duration between feature points of PPG, such as duration from the maximum derivative point to the dicrotic peak (Kim *et al* 2008), time span of cardiac cycle (Li *et al* 2014) and diastolic duration (Li *et al* 2014).
- Time relative indices: time ratio of systole to diastole (Li *et al* 2014) and large artery stiffness index (Kachuee *et al* 2017).

As is well known, BP is determined by CO and TPR. Among these PPG features, some were chosen according to their physiological mechanisms in relation to BP. For examples, the augmentation index is an indicator of wave reflection in arteries, the large artery stiffness index is a measure of arterial stiffness (Kachuee *et al* 2017, Slapničar *et al* 2018), and the ratio of PPG peak intensity to PPG valley intensity is related to the change in arterial diameter (Ding *et al* 2016). These features reflect the TPR and can therefore be used to estimate BP. Alternatively, time span indices decline and heart rate increases with the augmentation of cardiovascular workload during exercise (Li *et al* 2014), which affects CO and can therefore be used for BP estimation. The other features were selected by proving their correlation with BP values through data processing. For example, linear correlation analysis was conducted to find the features that were linearly related to BP in one of our previous studies (Lin *et al* 2018). Cross sample entropy and mutual information were used to find the PPG features that have a nonlinear relationship with BP in another previous study (Ding *et al* 2019). While a number of features were extracted from PPG waveforms, the underlying physiological mechanisms of the PPG features selected by data processing methods was unclear. Further investigation and understanding of the physiological mechanisms underlying these PPG features are critical. It is helpful to elucidate the intrinsic reasons why these PPG features could be used for better BP estimation and it would be beneficial to explore additional potential applications of these PPG features.

Therefore, this study aimed to investigate the physiological mechanisms of existing PPG features for BP estimation. To do so, two procedures, cold stimuli testing and an exercise trial, were conducted to change TPR and CO, respectively. This allowed us to investigate which features vary with TPR in the cold stimuli test and which features vary with CO in the exercise trial. The research outcomes of this work should shed light on the underlying physiological significance of these features.



2. Methods

2.1. Experiments

A total of 12 healthy subjects (aged 27.8 ± 5.4 years, BMI 22.4 ± 3.6 kg m⁻², weight 66.8 ± 13.0 kg, 2/12 female and 10/12 male) participated in the experiment. The whole experimental procedure included Phase 1 (baseline): the subject was instructed to sit on a chair quietly for 4.5 min, Phase 2 (cold stimuli): the subject remained seated on the chair and held a bottle full of ice for 3.5 min in their hand, then put down the bottle and kept quiet on the chair during recovery for 2.5 min, and Phase 3 (exercise): the subject left the chair and performed squat movements in place for 1 min, then sat back on the chair during quiet recovery for 1 min. Throughout the experiment, the PPG signal was continuously recorded by a Biopac® MP150 system PPG 100 C module at a sampling rate of 1000 Hz with the TSD 200 PPG sensor wrapped around the left index finger. The infrared wavelength of the TSD 200 PPG sensor used was $860 \text{ nm} \pm 60 \text{ nm}$. Meanwhile, the instantaneous left brachial BP was recorded by a commercial automatic BP meter (UOTT® Q6201, China) at the 60 s, 180 s, 270 s, 340 s, 410 s, 480 s, 550 s and 710 s time points of the experiment to record the fluctuations of BP. Before using the BP meter, the accuracy of the BP meter was double-checked by connecting to a mercurial sphygmomanometer synchronously using a T-branch pipe. The schematic diagram of the experimental procedure is shown in figure 2. The experimental protocol of the study was approved by the Shenzhen Institutes of Advanced Technology Institutional Review Board (SIAT-IRB-170315-H0150), Chinese Academy of Sciences, China, and written informed consent was obtained from all subjects.

2.2. Signal processing and data analysis

2.2.1. Signal preprocessing and feature points detection.

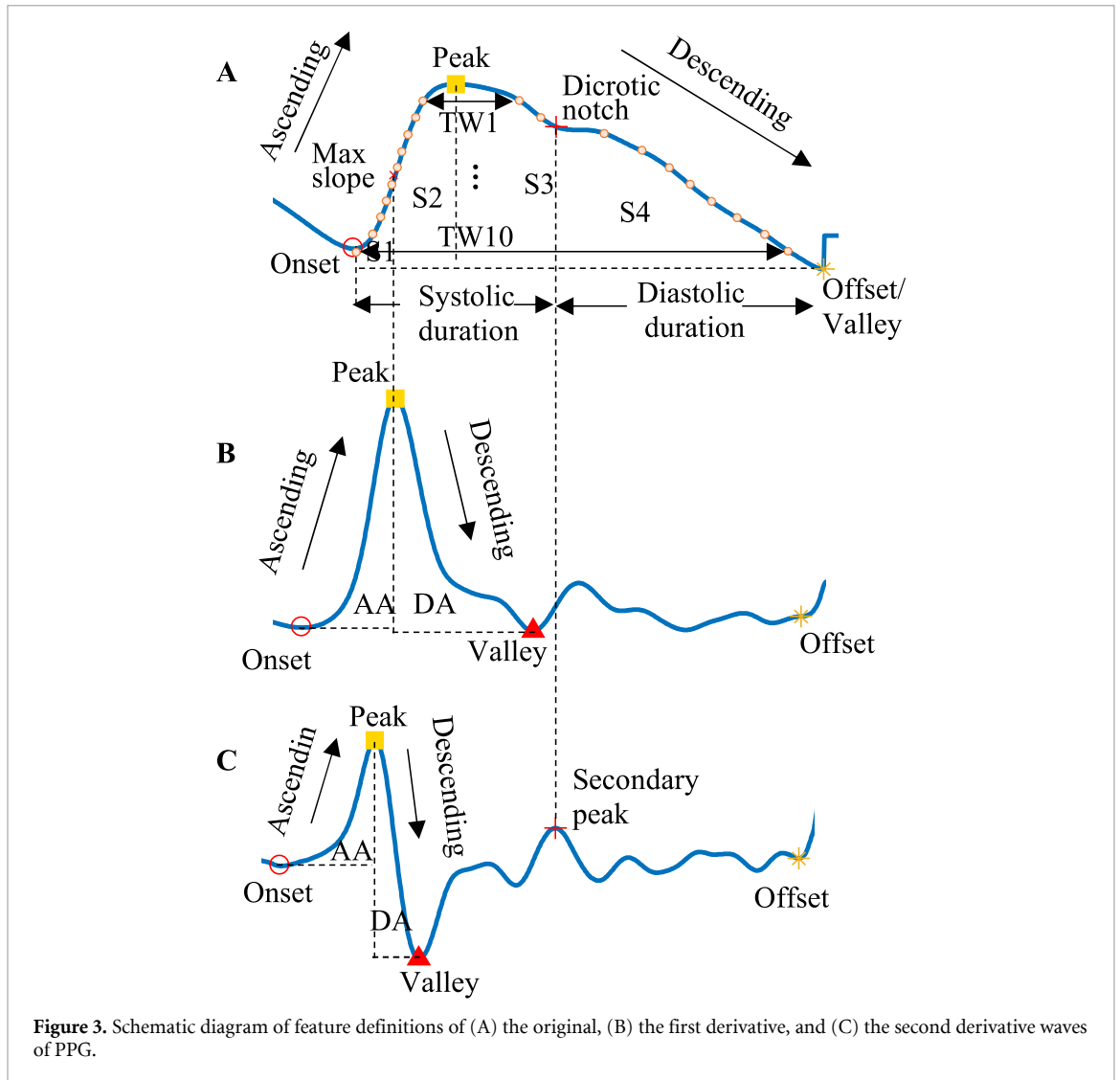
A novel algorithm for automatic detection of effective feature points was proposed in one of our previous studies (Lin et al 2019). The steps were briefly described as follows.

(1) Pre-processing.

The PPG signal was first pre-processed by a [0.05, 10] Hz, 4th-order Butterworth band-pass filter.

(2) Characteristic points detection and filtering.

A characteristic filtering algorithm was proposed to preserve the clean PPG cardiac cycles (with the characteristic points correctly identified) and to discard corrupted PPG cardiac cycles (with the characteristic points incorrectly identified due to excessive noise). Briefly, the characteristic points were detected first, including the main peak and the onset and offset of each PPG cardiac cycle. The main peak of each PPG cardiac cycle was detected through spline wavelet transform (Li et al 1995), based on the principle that the peak points correspond to the zero-crossing points of the maximum and minimum pairs in the 3rd scale of the wavelet transform, and then the onset and offset points of each PPG cardiac cycle were detected according to the points that had local minimum values, using the peak point as reference. After that, five characteristics, i.e. short-term energy (SE), ascending intensity difference (AID), descending intensity difference (DID), ascending time difference (ATD), and descending time difference (DTD), were chosen as metrics and calculated for each PPG cardiac cycle based on the characteristic points detected. Then the median lines of the five metrics were obtained using a median filter. An adaptive acceptable threshold around the median line of each metric was set based on histogram distribution analysis, where the histogram of the clean cardiac cycles was normally distributed but the histogram of the corrupted cardiac cycles was not. Therefore, the adaptive acceptable threshold could be used to examine pulse wave recordings on a



cardiac cycle-by-cycle basis. For each cardiac cycle, when one or more of its five characteristic values exceeded the acceptable range, that cardiac cycle was regarded as corrupted and excluded from further analysis. The results were double-checked manually. More details of the algorithm can be found in our previous study (Lin *et al* 2019). After the characteristic filtering, $44.0\% \pm 5.7\%$ cardiac cycles were kept across all subjects. Most of the cardiac cycles removed were those recorded during the exercise and cuff BP measurement, since exercise and cuff inflation can seriously distort the PPG wave.

(3) *Feature points detection in the original, the first derivative, and the second derivative waves of PPG.*

The preserved PPG wave after characteristic points filtering was normalized to values [0 1] using min-max normalization as in equation (1) for each subject:

$$x' = (x - X_{min}) / (X_{max} - X_{min}) \quad (1)$$

where x represents an element from a series of $\{X\}$, and X_{min} and X_{max} denote the minimum and maximum values of the PPG wave, respectively. Then the first derivative, and the second derivative waves of PPG were calculated and were also normalized to values [0 1]. Feature points in the original, the first derivative, and the second derivative waves of PPG, as shown in figure 3, were detected. It included the maximum peak, the onset and the offset points of the original, the first derivative and the second derivative waves of PPG, the valley points of the descending branch of the first derivative and the second derivative waves of PPG, and the secondary peak after the descending branch of the second derivative wave of PPG which were detected according to the points that had local maximum values or minimum values. In addition, the maximum slope of the ascending branch of the original PPG waveform was detected according to the maximum peak of the first derivative wave of PPG (Kachuee *et al* 2017), while the dicrotic notch of the original PPG waveform was also identified according to the secondary peak of the second derivative wave of PPG (Elgendi 2012).

Table 1. PPG feature definitions.

	Features	Definitions	Reference		
Slope indices	f1:Slope_a	Slope from maximum peak to dicrotic notch	Kim <i>et al</i> (2008)		
	f2:AS	Ascending slope (AS), i.e. slope from onset to maximum peak			
	f3:dAS		Descending slope (DS), i.e. slope from maximum peak to valley		
	f4:sdAS				
	f5:DS				
	f6:dDS				
	f7:sdDS				
Area indices	f8:S1	Area under the PPG curve between selected points (onset, max slope, maximum peak, and offset), as shown in figure 3.	Kachuee <i>et al</i> (2017)		
	f9:S2				
	f10:S3				
	f11:S4				
	f12:AA	Ascending area (AA), i.e. area under the curve from onset to maximum peak, as shown in figure 3.			
	f13:dAA	Descending area (DA), i.e. area under the curve from maximum peak to valley, as shown in figure 3.			
	f14:sdAA				
	f15:DA				
	f16:dDA				
	f17:sdDA				
	Area relative indices	f18: RtArea		Ratio of systolic area to diastolic area, i.e. $(S1 + S2 + S3)/S4$, as shown in figure 3.	Li <i>et al</i> (2014)
		f19:RAAD		Ratio of ascending area to descending area, i.e. AA/DA , as shown in figure 3.	
		f20:dRAAD			
		f21:sdRAAD			
f22:PI		Peak intensity (PI)			
Intensity indices	f23:dPI	Valley intensity (VI)	Fukushima <i>et al</i> (2013) Lin <i>et al</i> (2018)		
	f24:sdPI				
	f25:dVI				
	f26:sdVI				
	f27:NI			Dicrotic notch intensity (NI)	
	f28:AID			Ascending intensity difference (AID), i.e. intensity difference between onset and peak	
Intensity difference indices	f29:DID	Descending intensity difference (DID), i.e. intensity difference between peak and valley			
	f30:AI	Augmentation index (AI), i.e. ratio of dicrotic notch intensity to peak intensity	Kachuee <i>et al</i> (2017)		
f31:AI2	Augmentation index 2 (AI2), i.e. ratio of intensity difference between peak and dicrotic notch to peak intensity				
Intensity relative indices	f32:PIR	Photoplethysmogram intensity ratio (PIR), i.e. ratio of maximum peak intensity to onset intensity.	Ding <i>et al</i> (2016)		
	f33:dPIR	Ratio of maximum peak intensity to valley intensity (RIPV)			
	f34:sdPIR				
	f35:dRIPV				
	f36:sdRIPV				
	f37: PPG_k	PPG characteristic value	Miao <i>et al</i> (2017)		
	f38:TOO	Time interval between the onset of the second derivative wave of PPG and that of the first derivative wave of PPG			
	Time span indices	f39:AT	Ascending time (AT), i.e. time span from onset to peak	Wang <i>et al</i> (2016)	
f40:DT		Descending time (DT), i.e. time span from maximum peak to valley			
f41:dDT					
f42:sdDT					
f43:CC		Cardiac cycle (CC), i.e. time span from onset to offset.	Lin <i>et al</i> (2015)		
f44:dCC					
f45:sdCC					
f46:dTVO		Time span from valley to offset (TVO)			
f47:sdTVO					

Table 1. (continued)

	Features	Definitions	Reference
	f48:SD f49:sdSD f50:DD	Systolic duration (SD), i.e. time duration from onset to dicrotic notch	Lin <i>et al</i> (2015)
	f51:sdDD	Diastolic duration (DD), i.e. time duration from dicrotic notch to offset	
	f52:TW1 f53:TW2 f54:TW3 f55:TW4 f56:TW5 f57:TW6 f58:TW7 f59:TW8 f60:TW9 f61:TW10	Time width at 10/11, 9/11, 8/11, 7/11, 6/11, 5/11, 4/11, 3/11, 2/11, 1/11 of pulse amplitude of the PPG waveform, respectively.	Teng <i>et al</i> (2003)
Time relative indices	f62:RSD	Ratio of systolic duration to diastolic duration (RSD), i.e. SD/DD	Lin <i>et al</i> (2015)
	f63:RSC	Ratio of systolic duration to cardiac cycle (RSC), i.e. SD/CC	
	f64:RDC	Ratio of diastolic duration to cardiac cycle (RDC), i.e. DD/CC	
	f65:LASI	Large Artery Stiffness Index (LASI), i.e. inversely related to the time interval between peak and dicrotic notch	Kachuee <i>et al</i> (2017)

The prefix 'd' indicates that the feature was extracted from the first derivative wave of PPG, prefix 'sd' indicates that the feature was calculated from the second derivative wave of PPG, while no prefix indicates that the feature was computed from the original PPG wave.

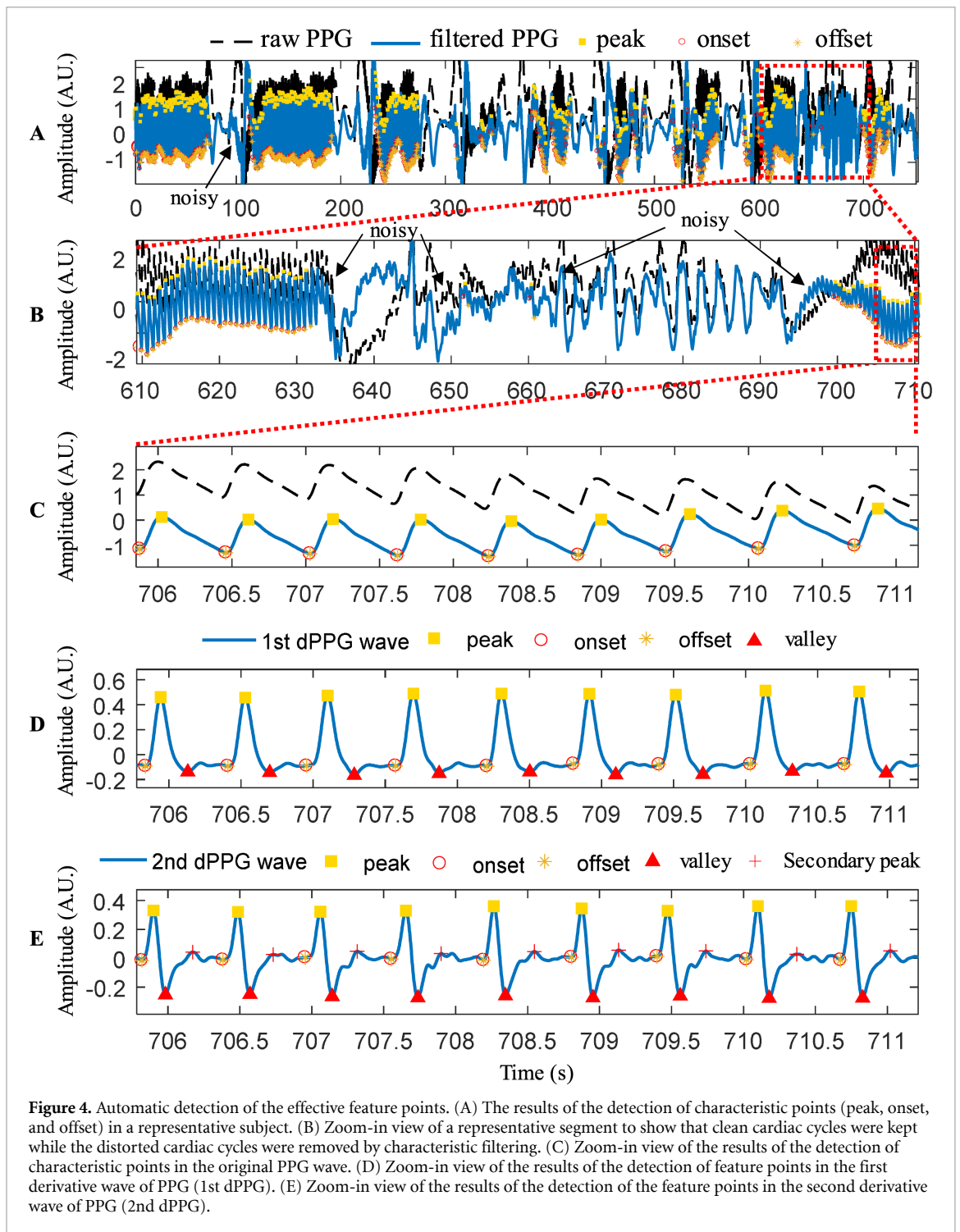
2.2.2. PPG features definition.

According to the definitions in table 1, a total of 65 PPG features were calculated from the original, the first derivative, and the second derivative waves of PPG, including those used in previous studies and those proved useful for BP estimation in our studies. The types of features included (1) slope indices, (2) area indices, (3) area relative indices, (4) intensity indices, (5) intensity difference indices, (6) intensity relative indices, (7) time span indices, and (8) time relative indices. The schematic diagram of the definitions of several important PPG features is shown in figure 3.

2.2.3. Statistical analysis.

The instantaneous BP values were recorded eight times to observe the fluctuation of BP during the experiment. Four groups of instantaneous BP values in the middle baseline phase (180 s), the peak cold stimuli period (410 s), the end of cold recovery period (550 s), and the early exercise recovery period (710 s), as shown in figure 2, were selected for analysis. BP in the middle baseline phase (180 s) was chosen as the representative of the baseline period since the state of the subject was relatively stable at this time. The peak cold stimuli period (410 s) was chosen to study the highest reaction of the cold stimuli. BP at the end of cold recovery period (550 s) was analyzed to investigate whether the cold recovery period was long enough for the cardiovascular system to return to the baseline level. The early exercise recovery period (710 s) was used to study the response of the cardiovascular parameters to exercise. Mean \pm SD (standard deviation) of the systolic BP (SBP) and diastolic BP (DBP) values were calculated across all subjects for each selected period.

The mean values of each PPG feature in the whole baseline phase (0–270 s), the cold stimuli phase (270–480 s), and the early exercise recovery period (690–750 s) were calculated, respectively. Data from the early exercise recovery period (within 1 min immediately after the cessation of exercise) were used instead of those in the exact exercise period to study the response of the cardiovascular parameters to exercise, since data in the exact exercise period were too noisy to be correctly analyzed, and the cardiovascular variables in the early exercise recovery period had not yet returned to the baseline level. Mean \pm SD values of each feature were calculated across all subjects for each selected period. Differences between BP/PPG feature values in the baseline phase and those in other periods were assessed using Student's *t*-test. A *p*-value < 0.05 was considered statistically significant.



3. Results

3.1. Feature points detection

Figure 4 shows the results of the feature points detection in the original, the first and the second derivative waves of PPG in a representative segment. The cardiac cycles whose feature points were incorrectly identified because of too much noise were automatically discarded from further analysis, as can be seen in figures 4(A) and (B), while the clean cardiac cycles with the feature points automatically and accurately detected were used for further feature extraction and statistical analysis, as can be seen in figures 4(C)–(E).

3.2. Fluctuations of BP and PPG features in a subject

Figure 5 shows the fluctuations of the instantaneous BP and extracted PPG features during the whole experiment in a representative subject. BP values increased obviously in the cold stimuli phase, reached

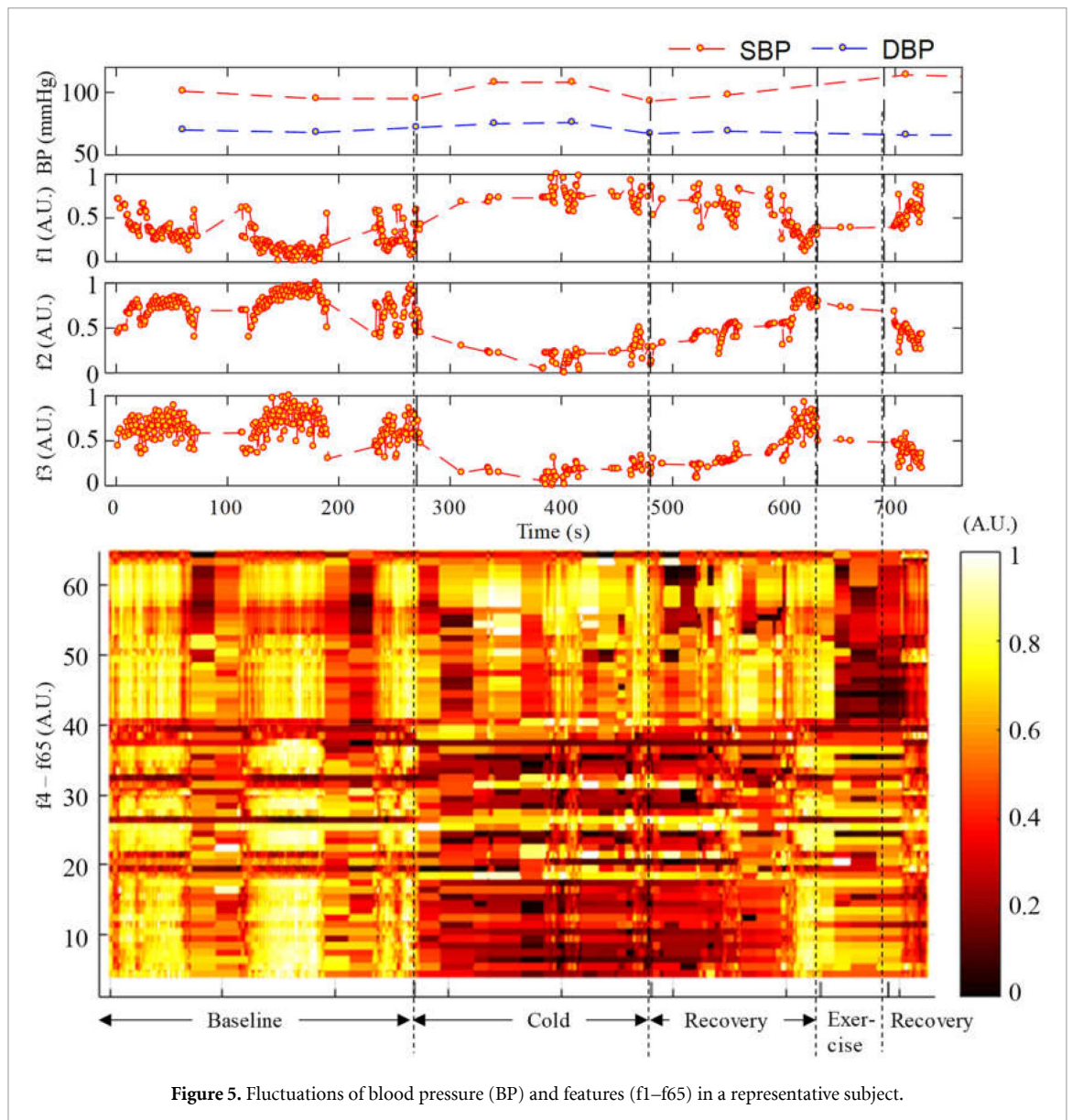
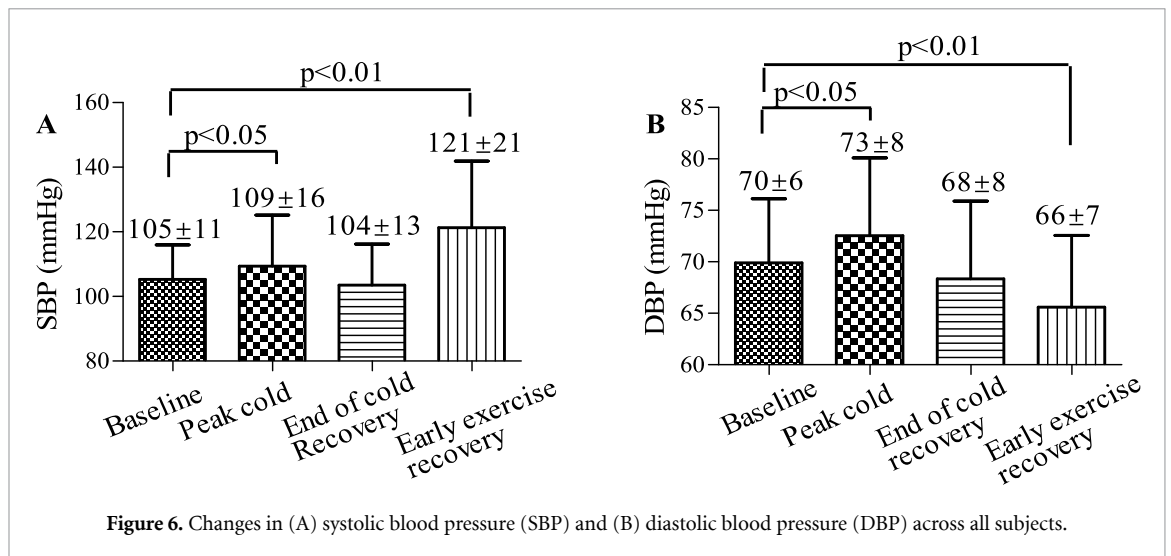


Figure 5. Fluctuations of blood pressure (BP) and features (f1–f65) in a representative subject.

a peak over a period of cold stimuli (near 410 s), and slowly returned to baseline level at the end of the cold recovery period. Exercise also induced an elevation in BP. BP measured immediately after the cessation of exercise (i.e. the early exercise recovery period) also increased obviously. These observations indicated that the intensity of the cold stimulus and exercise was sufficient to elicit an obvious cardiovascular physiological response in the subject. In order to better show the fluctuating trends of the features with external condition, only the first three features (f1–f3) were plotted in detail, while the other features (f4–f65) were represented by a pseudocolor plot. Spline interpolation and normalization were carried out for each feature value series before plotting. It can be seen from the figure that some features (most of the features between f1–f40) changed obviously in the cold stimuli phase and returned to baseline level at the end of the cold recovery period, indicating that these features were related to the TPR, while some features (most of the features between f41–f65) changed obviously in the exercise phase, indicating that these features were closely related to CO.

3.3. Changes in BP and PPG features across all subjects

Figure 6 shows the mean \pm SD of BP values in selected representative periods across all subjects. BP values in the peak cold stimuli period (410 s) and the early exercise recovery period (710 s) were significantly higher ($p < 0.05$) compared with the baseline period (180 s), indicating that the intensity of the cold stimulus and exercise was sufficient to elicit an obvious cardiovascular physiological response across all subjects. BP values at the end of the cold recovery period (550 s) showed no significant difference from the baseline period



(180 s), indicating that the cold recovery period was long enough for the cardiovascular system to be restored to the baseline level across all subjects.

Table 2 presents the mean \pm SD of PPG feature values in different experimental periods across all subjects. As seen in the table, the PPG features in the cold stimuli phase showed significant differences ($p < 0.05$) from those in the baseline phase (including all of the slope indices, all of the area indices, one of the area relative indices, most of the intensity indices, all of the intensity difference indices, and most of the intensity relative indices). Cold stimuli can cause peripheral vascular contraction and lead to the increase of TPR. Thus, these PPG features were TPR-correlated. The PPG features in the early exercise recovery period showed significant differences ($p < 0.05$) from those in the baseline phase (including most of the time span indices, most of the time relative indices, some area relative indices, some area indices, and one of the slope indices). Exercise can increase the heart rate and CO. Thus, these PPG features were CO-correlated. PPG features f5: DS, f11: S4, f15: DA extracted from the descending branch of the PPG wave fluctuated significantly both in the cold stimuli phase and the early exercise recovery period. Thus, these PPG features were both TPR-correlated and CO-correlated.

4. Discussion and conclusion

In order to investigate the physiological mechanism of the existing commonly used PPG features used for BP estimation, two procedures (i.e. cold stimuli and exercise trial) were conducted to change the TPR and CO, respectively, in this work. The main findings in this work were as follows. All of the slope indices, all of the area indices, one of the area relative indices, most of the intensity indices, all of the intensity difference indices, and most of the intensity relative indices showed significant fluctuations during the cold stimuli phase when compared with the baseline phase, indicating that these features were TPR-correlated. Most of the time span indices, most of the time relative indices, some area relative indices, some area indices, and one of the slope indices showed significant fluctuations in the early exercise recovery period when compared with the baseline phase, indicating that these features were CO-correlated. PPG features in terms of slope and area, especially those extracted from the descending branch of the PPG wave, fluctuated significantly both in cold stimuli phase and in the early exercise recovery period, indicating that these features were both TPR-correlated and CO-correlated. As is well known, BP could be determined as a product of CO and TPR. This study demonstrated that the examined PPG features were TPR-correlated and/or CO-correlated, which can largely explain the intrinsic physiological mechanisms by which these features could be applied to BP estimation. It also helps to explore more potential applications of these PPG features.

4.1. Physiological mechanism analysis of the TPR-correlated PPG features

During the cold stimuli phase, BP increased with muscle sympathetic activity, and vasoconstriction led to a significant increase in TPR; but the small increase in heart rate in the early cold stimuli period (about 30 s) may be abolished by beta-adrenergic blockade later on (Victor *et al* 1987). Figure 7(A) shows the changes of heart rate in a representative subject, and figure 7(B) shows the statistical analysis results across all subjects. There was no significant change in heart rate compared with baseline during cold stimulation or cold recovery periods in this experiment. Thus, the CO would not change too much in the cold stimuli phase. Since a typical PPG wave contour is a mixture of both the forward wave (generated by CO) and the reflected

Table 2. PPG feature values in different experimental periods across the subjects.

	Features	Baseline (Mean \pm SD)	Cold stimuli (Mean \pm SD)	Early exercise recovery (Mean \pm SD)	Correlated
Slope indices	f1:Slope_a	-0.62 ± 0.29^c	-0.46 ± 0.22^c	-0.67 ± 0.27	TPR
	f2:AS	1.97 ± 0.66^c	1.54 ± 0.54^c	2.03 ± 0.64	TPR
	f3:dAS	4.68 ± 1.12^c	3.74 ± 1.10^c	4.57 ± 1.81	TPR
	f4:sdAS	3.39 ± 0.83^c	2.68 ± 0.68^c	3.45 ± 1.39	TPR
	f5:DS	$0.48 \pm 0.18^{c,a}$	0.39 ± 0.15^c	0.58 ± 0.19^a	TPR, CO
	f6:dDS	6.35 ± 2.09^c	4.91 ± 2.07^c	6.79 ± 2.71	TPR
	f7:sdDS	7.84 ± 2.12^c	6.42 ± 2.08^c	8.42 ± 3.07	TPR
Area indices	f8:S1	3.61 ± 1.33^c	2.80 ± 1.14^c	3.34 ± 1.26	TPR
	f9:S2	21.33 ± 10.47^c	17.80 ± 9.19^c	18.61 ± 7.79	TPR
	f10:S3	42.23 ± 14.20^c	33.90 ± 14.19^c	33.97 ± 14.62	TPR
	f11:S4	$49.94 \pm 14.09^{c,b}$	44.40 ± 15.35^c	35.01 ± 12.19^b	TPR, CO
	f12:AA	24.97 ± 11.41^c	20.57 ± 10.02^c	21.78 ± 8.92	TPR
	f13:dAA	23.54 ± 6.75^c	19.41 ± 6.99^c	24.43 ± 7.75	TPR
	f14:sdAA	10.86 ± 3.18^c	8.96 ± 3.13^c	10.83 ± 3.19	TPR
	f15:DA	$92.36 \pm 25.01^{c,b}$	79.55 ± 25.37^c	71.87 ± 26.20^b	TPR, CO
	f16:dDA	20.14 ± 6.13^c	17.01 ± 6.71^c	19.38 ± 6.44	TPR
	f17:sdDA	22.94 ± 6.38^c	18.03 ± 6.65^c	23.27 ± 7.33	TPR
Area relative indices	f18: RtArea	0.78 ± 0.16	0.83 ± 0.19	0.69 ± 0.19	—
	f19:RAAD	0.26 ± 0.07^a	0.25 ± 0.07	0.30 ± 0.05^a	CO
	f20:dRAAD	1.18 ± 0.16^a	1.16 ± 0.17	1.27 ± 0.07^a	CO
	f21:sdRAAD	0.47 ± 0.03^c	0.50 ± 0.02^c	0.47 ± 0.03	TPR
Intensity indices	f22:PI	0.65 ± 0.05	0.63 ± 0.07	0.63 ± 0.08	—
	f23:dPI	0.76 ± 0.08^c	0.67 ± 0.07^c	0.76 ± 0.11	TPR
	f24:sdPI	0.82 ± 0.08^c	0.76 ± 0.06^c	0.83 ± 0.07	TPR
	f25:dVI	0.29 ± 0.12	0.29 ± 0.12	0.29 ± 0.12	—
	f26:sdVI	0.22 ± 0.09^c	0.28 ± 0.11^c	0.20 ± 0.16	TPR
	f27:NI	0.55 ± 0.05	0.55 ± 0.05	0.53 ± 0.05	—
	f28:AID	0.30 ± 0.10^c	0.24 ± 0.08^c	0.29 ± 0.10	TPR
Intensity difference indices	f29:DID	0.31 ± 0.10^c	0.25 ± 0.08^c	0.29 ± 0.09	TPR
	f30:AI	0.32 ± 0.05	0.29 ± 0.06	0.33 ± 0.07	—
Intensity relative indices	f31:AI2	0.68 ± 0.05	0.71 ± 0.06	0.66 ± 0.07	—
	f32:PIR	1.96 ± 0.45^c	1.67 ± 0.32^c	1.78 ± 0.35	TPR
	f33:dPIR	3.94 ± 1.39^c	3.40 ± 1.27^c	4.19 ± 1.58	TPR
	f34:sdPIR	1.64 ± 0.17^c	1.52 ± 0.17^c	1.65 ± 0.23	—
	f35:dRIPV	2.92 ± 0.78^c	2.62 ± 0.78^c	2.93 ± 0.89	TPR
	f36:sdRIPV	4.97 ± 3.00^c	3.19 ± 1.55^c	5.61 ± 3.59	TPR
	f37: PPG_k	$0.49 \pm 0.07^{c,a}$	0.52 ± 0.08^c	0.54 ± 0.14^a	TPR, CO
	f38:TOO	0.02 ± 0.01^b	0.02 ± 0.00	0.01 ± 0.01^b	CO
Time span indices	f39:AT	0.16 ± 0.04	0.16 ± 0.04	0.14 ± 0.02	—
	f40:DT	0.65 ± 0.06^b	0.64 ± 0.08	0.50 ± 0.05^b	CO
	f41:dDT	0.69 ± 0.09^b	0.69 ± 0.10	0.53 ± 0.05^b	CO
	f42:sdDT	0.71 ± 0.09^b	0.71 ± 0.10	0.56 ± 0.06^b	CO
	f43:CC	0.81 ± 0.10^b	0.80 ± 0.10	0.64 ± 0.06^b	CO
	f44:dCC	0.81 ± 0.10^b	0.80 ± 0.11	0.65 ± 0.08^b	CO
	f45:sdCC	0.81 ± 0.10^b	0.80 ± 0.10	0.65 ± 0.08^b	CO
	f46:dTVO	0.60 ± 0.06^b	0.59 ± 0.08	0.46 ± 0.04^b	CO
	f47:sdTVO	0.63 ± 0.09^b	0.63 ± 0.10	0.48 ± 0.05^b	CO
	f48:SD	0.32 ± 0.07	0.32 ± 0.07	0.28 ± 0.04	—
	f49:sdSD	0.38 ± 0.07^a	0.38 ± 0.07	0.35 ± 0.05^a	CO
	f50:DD	0.48 ± 0.05^b	0.48 ± 0.05	0.36 ± 0.03^b	CO
	f51:sdDD	0.42 ± 0.04^b	0.42 ± 0.05	0.31 ± 0.03^b	CO
	f52:TW1	98.33 ± 27.39	101.82 ± 27.65	81.87 ± 20.58	—
f53:TW2	157.35 ± 52.28	162.88 ± 51.91	127.23 ± 22.79	—	
f54:TW3	213.20 ± 67.74^a	227.82 ± 67.74	166.69 ± 26.45^a	CO	
f55:TW4	284.20 ± 71.15^b	300.24 ± 73.08	205.28 ± 37.95^b	CO	
f56:TW5	369.21 ± 49.65^b	366.65 ± 51.85	254.69 ± 51.06^b	CO	
f57:TW6	418.46 ± 50.42^b	413.11 ± 55.88	324.63 ± 58.66^b	CO	
f58:TW7	465.98 ± 58.46^b	460.16 ± 62.84	372.97 ± 52.61^b	CO	
f59:TW8	517.97 ± 66.48^b	510.55 ± 71.20	420.50 ± 51.98^b	CO	
f60:TW9	577.89 ± 73.62^b	567.55 ± 79.93	469.99 ± 53.65^b	CO	
f61:TW10	650.94 ± 80.48^b	635.10 ± 89.23	521.67 ± 56.28^b	CO	

Table 2. (continued)

	Features	Baseline (Mean \pm SD)	Cold stimuli (Mean \pm SD)	Early exercise recovery (Mean \pm SD)	Correlated
Time relative indices	f62:RSD	1.53 \pm 0.21 ^a	1.54 \pm 0.24	1.30 \pm 0.20 ^a	CO
	f63:RSC	0.40 \pm 0.04 ^b	0.40 \pm 0.04	0.44 \pm 0.03 ^b	CO
	f64:RDC	0.60 \pm 0.04 ^b	0.60 \pm 0.04	0.56 \pm 0.03 ^b	CO
	f65:LASI	6.18 \pm 0.90	6.42 \pm 1.17	7.66 \pm 2.88	—

^a $p < 0.05$ indicates that the differences between values in baseline phase and those in exercise phase were statistically significant at the level 0.05.

^b $p < 0.01$ indicates that the differences between values in baseline phase and those in exercise phase were statistically significant at the level 0.01.

^c $p < 0.01$ indicates that the differences between values in baseline phase and those in cold stimuli phase were statistically significant at the level 0.01.

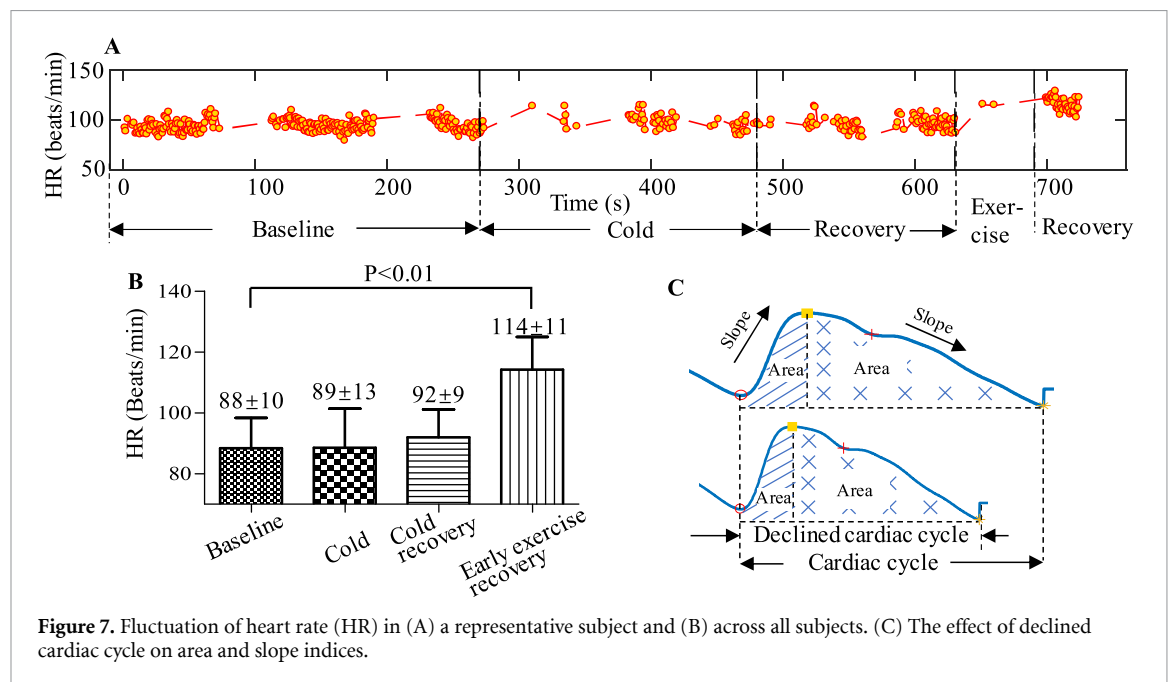


Figure 7. Fluctuation of heart rate (HR) in (A) a representative subject and (B) across all subjects. (C) The effect of declined cardiac cycle on area and slope indices.

wave (generated by the TPR), an increase in the TPR with constant CO will increase the reflected wave and thus would influence the PPG features associated with intensity, slope, and area. This could explain the statistical analysis results of this study, in which features including all of the slope indices, all of the area indices, one of the area relative indices, most of the intensity indices, all of the intensity difference indices, and most of the intensity relative indices changed significantly in the cold stimuli phase when compared with the baseline. Thus, it can be concluded that PPG features associated with intensity, slope, and area were TPR-correlated.

4.2. Physiological mechanism analysis of the CO-correlated PPG features

During the early exercise recovery period, sympathetic tone also increased when compared with the baseline phase, but unlike during the cold stimuli phase, a dramatic increase in heart rate, as shown in figures 7(A) and (B), led to an increase in CO and a decline in time span indices when compared with the baseline phase. This was consistent with the statistical analysis results of this study, in which most of the time span indices and most of the time relative indices changed significantly in the early exercise recovery period when compared with the baseline. Thus, it can be concluded that PPG features associated with time were CO-correlated.

In further analysis, the decline in cardiac cycle would also influence the features associated with slope and area, as shown in figure 7(C). Thus some features associated with slope and area also showed significant differences in the early exercise recovery period when compared with the baseline phase, especially the features extracted from the descending branch of the PPG wave f5: DS, f11: S4, f15: DA, suggesting that these features were also CO-correlated. Although other PPG features associated with slope and area showed no significant difference in the early exercise recovery period, they also showed obvious changes when compared

with the baseline phase from the data. The reason for the lack of statistically significant differences may be that the intensity of exercise was not strong enough to induce significant responses in these features. However, it can be concluded that PPG features associated with slope and area were not only TPR-correlated, but may also be CO-correlated.

It is worth noting that in previous studies (e.g. Kachuee *et al* 2017), the large artery stiffness index f65: LASI was a measure of arterial stiffness. In this study, although the changes in LASI showed no significant difference in the cold stimuli phase when compared with the baseline level, the data showed obvious changes both in the cold stimuli and in the early exercise recovery period, indicating that it might be both TPR-correlated and CO-correlated. According to the definition, LASI is inversely related to the time interval between peak and dicrotic notch. The dicrotic notch is produced by reflected waves generated by TPR, so PPG features associated with the dicrotic notch may be TPR-correlated. In addition, time indices were CO-correlated according to the analysis mentioned above. Thus, time indices associated with the dicrotic notch may be both TPR-correlated and CO-correlated.

One limitation of this study is that the intensity of exercise might not have been strong enough to induce statistically significant responses of the features associated with slope and area compared with the baseline level. Another limitation of this study is that the subjects were all healthy people; however, the contours of the PPG wave in patients, especially in hypo- or hypertensive patients, are quite different from those in healthy people. Therefore, the results of this study need to be verified and discussed in patients in future work.

In summary, the present work investigated the physiological mechanisms of the PPG features for BP estimation. We found that PPG features associated with intensity were TPR-correlated, those features associated with time were CO-correlated, and those features associated with slope and area may be both TPR-correlated and CO-correlated. The findings largely explained the intrinsic physiological mechanisms by which these features could be applied to BP estimation. As is well known, the aim of PPG-based BP estimation is for wearable, real-time and long-term monitoring, so the cardiovascular state (e.g. TPR, CO) of the patients would vary greatly under different application scenarios (e.g. temperature, exercise). This would influence the relationships between PPG features and BP and would affect the accuracy of BP estimation, especially when the measurement condition is different from the calibration condition. However, if we know the physiological mechanisms of the PPG features, we can include the corresponding features into the BP estimation model to track changes in cardiovascular state for specific conditions, which can improve the robustness of the BP estimation model.

Acknowledgments

This work was partially supported by National Natural Science Foundation of China under Grant Nos. #61901461, #61803361, #U1613222, National Key R&D Program of China (Grant Nos. 2019YFC1710400; 2019YFC1710402), The Ministry of Science and Technology of the People's Republic of China (Grant No. 2016YFE0124100), Shenzhen Governmental Collaborative Innovation Program (Grant No. #SGLH20180625142402055), Shenzhen Institute of Artificial Intelligence and Robotics for Society, and Shenzhen Basic Research Grant (Grant No. JCYJ20170818163724754).

Funding

Shenzhen Institute of Artificial Intelligence and Robotics for Society.

Conflict of interest

All the authors declare that there is no financial relationship with any product, service, or company mentioned in this paper.

ORCID iDs

Wan-Hua Lin  <https://orcid.org/0000-0002-8953-8469>

Fei Chen  <https://orcid.org/0000-0002-6988-492X>

References

Ding X R, Yan B P, Zhang Y T, Liu J, Su P and Zhao N 2019 Feature exploration for knowledge-guided and data-driven approach based cuffless blood pressure measurement *Electr. Eng. Syst. Sci.: Signal Process.* **1908** 1–4 <https://arxiv.org/abs/1908.10245>

- Ding X R, Zhang Y T, Liu J, Dai W X and Tsang H K 2016 Continuous cuffless blood pressure estimation using pulse transit time and photoplethysmogram intensity ratio *IEEE Trans. Biomed. Eng.* **63** 964–72
- Elgendi M 2012 On the analysis of fingertip photoplethysmogram signals *Curr. Cardiol. Rev.* **8** 14–25
- Fukushima H, Kawanaka H, Bhuiyan M S and Oguri K 2013 Cuffless blood pressure estimation using only photoplethysmography based on cardiovascular parameters *35th Annual Int. Conf. of the IEEE Engineering in Medicine and Biology Society (EMBC) (Osaka, Japan)* pp 2132–5
- Kachuee M, Kiani M M, Mohammadzade H and Shabany M 2017 Cuffless blood pressure estimation algorithms for continuous health-care monitoring *IEEE Trans. Biomed. Eng.* **64** 859–69
- Kim J S, Kim K K, Baek H J and Park K S 2008 Effect of confounding factors on blood pressure estimation using pulse arrival time *Physiol. Meas.* **29** 615–24
- Li C W, Zheng C X and Tai C F 1995 Detection of Ecg characteristic points using wavelet transforms *IEEE Trans. Biomed. Eng.* **42** 21–28
- Li Y, Wang Z, Zhang L, Yang X and Song J 2014 Characters available in photoplethysmogram for blood pressure estimation: beyond the pulse transit time *Australas. Phys. Eng. Sci. Med.* **37** 367–76
- Lin H, Xu W Y, Guan N, Ji D, Wei Y J and Yi W 2015 Noninvasive and continuous blood pressure monitoring using wearable body sensor networks *IEEE Intell. Syst.* **30** 38–48
- Lin W H, Ji N, Wang L and Li G L 2019 A characteristic filtering method for pulse wave signal quality assessment *41st Annual Int. Conf. of the IEEE Engineering in Medicine and Biology Society (EMBC) (Berlin, Germany)* pp 603–6
- Lin W H, Wang H, Samuel O W, Liu G, Huang Z and Li G 2018 New photoplethysmogram indicators for improving cuffless and continuous blood pressure estimation accuracy *Physiol. Meas.* **39** 025005
- Liu Q, Yan B P, Yu C M, Zhang Y T and Poon C C 2014 Attenuation of systolic blood pressure and pulse transit time hysteresis during exercise and recovery in cardiovascular patients *IEEE Trans. Biomed. Eng.* **61** 346–52
- Miao F, Fu N, Zhang Y T, Ding X R, Hong X, He Q and Li Y 2017 A novel continuous blood pressure estimation approach based on data mining techniques *IEEE J. Biomed. Health Inform.* **21** 1730–40
- Mukkamala R, Hahn J O, Inan O T, Mestha L K, Kim C S, Töreyn H and Kyal S 2015 Toward ubiquitous blood pressure monitoring via pulse transit time: theory and practice *IEEE Trans. Biomed. Eng.* **62** 1879–901
- Proença M, Renevey P, Braun F, Bonnier G, Delgado-Gonzalo R Lemkaddem A et al 2019 Pulse wave analysis techniques *The Handbook of Cuffless Blood Pressure Monitoring*, ed J Solà and R Delgado-Gonzalo (Cham: Springer) pp 107–37
- Putyatina Y S 2002 Measurement of arterial blood pressure by processing pulse wave data *3rd Annual 2002 Siberian Russian Workshop on Electron Devices and Materials (Erlagol, Russia)* pp 77–78
- Slapničar G, Luštrek M and Marinko M 2018 Continuous blood pressure estimation from PPG signal *Informatica* **42** 33–42 (<http://www.informatica.si/index.php/informatica/article/view/2229/1146>)
- Teng X F and Zhang Y T 2003 Continuous and noninvasive estimation of arterial blood pressure using a photoplethysmographic approach *25th Annual Int. Conf. of the IEEE Engineering in Medicine and Biology Society (EMBC) (Cancun, Mexico)* pp 3153–6
- Victor R G, Leimbach W N Jr., Seals D R, Wallin B G and Mark A 1987 Effects of the cold pressor test on muscle sympathetic nerve activity in humans *Hypertension* **9** 429–36
- Wang M, Huang C, Chen H and Ye S 2016 Preprocessing PPG and ECG signals to estimate blood pressure based on noninvasive wearable device *3rd Int. Conf. on Engineering Technology and Application (ICETA 2016) (Kyoto, Japan)* pp 1103–6